HYDRODYNAMICS IN A DISPOSABLE RECTANGULAR PARALLELEPIPED STIRRED BIOREACTOR WITH ELLIPTIC PENDULUM MOTION PADDLE

Marie-Laure Collignon [a, b,1], Laurent Droissart [a], Angélique Delafosse [a], Sebastien Calvo [a], Steven Vanhamel [c], Roman Rodriguez [c], Tom Claes [c], Fabien Moncaubeig [d], Ludovic Peeters [e], Michel Crine [a,b], Dominique Toye [a]

[a] Laboratory of Chemical Engineering, University of Liège, Sart-Tilman, B6, B4000 Liège, Belgium

[b] F.R.S.-FNRS, Rue d'Egmont 5, B1000 Bruxelles, Belgium

[c] ATMI LifeSciences, Reugelstraat 2, B3320 Hoegaarden, Belgium

[d] Artelis, rue de Ransbeek 310, B1120 Bruxelles, Belgium

[e] GlaxoSmithKline Biologicals, rue de l'Institut 89, B1330 Rixensart, Belgium

Abstract

Stainless steel bioreactors increasingly give way to their disposable counterparts in pharma research as no cleaning or sterilisation is required. This led company ATMI LifeSciences to develop the "Nucleo^{TM}". Original in design, this disposable bioreactor comprises a rectangular parallelepiped plastic bag stirred by a paddle revolving in elliptic pendulum motion. Studies covering this bioreactor showed good homogeneity of culture medium as well as good productivity for animal cell cultures. To further explain these good performances, the flow inside the "Nucleo^{TM}" must be resolved. This paper focuses on the mean flow description, computed from stereo-PIV measurements performed in 20 vertical covering the whole volume of a 50 dm³ Nucleo^{TM} bioreactor. As the flow is already turbulent in the chosen agitation conditions, its dimensionless mean velocity field does not vary with the paddle rotational speed. Mean flow pattern exhibits an axial symmetry – same flow is observed in opposite quarters of the tank – and can be described as a three-dimensional helix coiled on itself to form a distorted horizontal torus which covers the whole tank volume. Mean velocity is on average twice higher in the cone swept by the paddle and its two horizontal components are twice the vertical one. However, mean velocity remains significant everywhere and, in particular, no stagnant area is observed in tank corners. Above outcomes thus confirm previous studies observations.

[1] Corresponding author: Tel: +32 4 366 47 22 – Fax:+32 4 366 28 18
E-mail: mlcollignon@ulg.ac.be

Keywords: Agitation, animal cell culture, bioprocess design, fluid mechanics, stereo-PIV, mean flow characterisation.

1. Introduction

In recent years, a significant shift towards disposable bioreactors occurred in pharma research. Dedicated to one animal cell culture, they usually comprise a closed and sterile plastic bag attached to a steel structure and equipped with connections for introducing culture medium and various probes. As their use brings many benefits, they have been gradually replacing their steel counterparts [1]. The most obvious advantage is removing two costly steps, i.e. washing and sterilisation between production campaigns, which in turn reduces global environmental impact in spite of higher solid waste [2]. Other major strategic advantages are a significant reduction in time required to build and validate a new production facility together with higher flexibility in the production capacity [2].

Recognizing high potential in this market, many companies developed disposable bioreactors, such as the SUB (Hyclone), the Xcellerex (XDR) or the BioStat STR (Sartorius Stedim) amongst stirred versions, which hold to the conventional geometry of steel devices. Others have original design. It is the case of the disposable bioreactor studied in this paper, the Nucleo^{TM} bioreactor commercialized by ATMI LifeSciences. As illustrated in Figure 1, device comprises a rectangular parallelepiped plastic bag stirred by a paddle integrated in the bag and covered by the same multilayer polymer. When oxygen supply is required, a sparger is fitted at the lower end of the blade. The bag rests in a stainless steel frame. The blade is connected to the motor through a metal rod which fits into the hollow axis of the blade. The blade is inclined at 13.5° with respect to the vertical and therefore draws an elliptical pendulum trajectory in the vessel, as illustrated in Figure 2. The motion of the paddle through the bag can be visualized in the video available on the electronic version of this paper. The bag is equipped with several disposable sensors (pH, dissolved O_2, etc.) and with several sterile connections to enable gas injection and exhaust, to add the culture medium or for sampling.

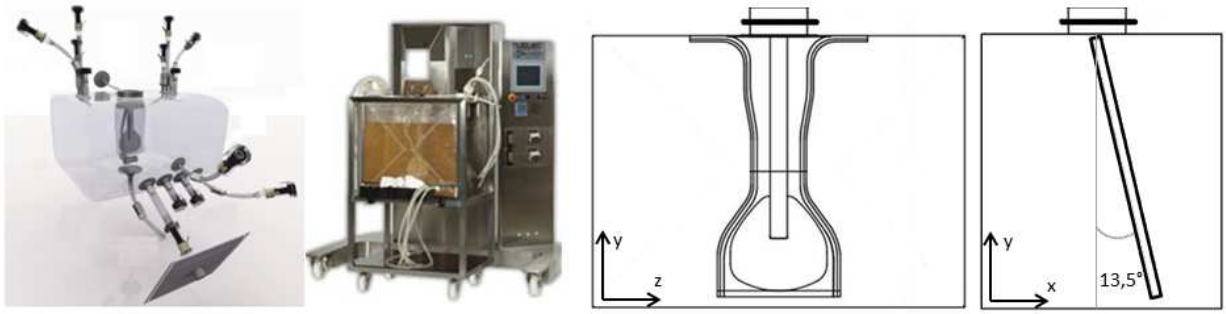

Figure 1: Design of the Nucleo^{TM} disposable bioreactor.

This original stirred bioreactor is a joint development by companies ATMI LifeSciences, Pierre Guerrin and Artelis, which aims at a better answer to specific requirements of animal cell culture. Indeed, as other microorganisms, animal cells require a constant physico-chemical environment, which means good homogenisation and aeration of the culture medium. However, unlike bacteria or yeast, animal cells do not possess a rigid cell wall but a fragile plasma membrane, which leads to consider them as particularly shear-sensitive. Mechanical constraints generated inside the culture medium due to its mixing and aeration must thus be as small as possible [3] [4]. Fulfilling these two opposite requirements becomes even more of a challenge in anchorage-dependent cell culture, *i.e.* when cells are fixed on the surface of microcarriers. So as to maximize surface available for cell development, the latter must remain in complete suspension in the culture medium but will also collide with each other, thus creating additional mechanical constraints.

Studies show that the Nucleo^{TM}, thanks to its original design, reconciles (i) liquid and solid homogenisation and (ii) minimising mechanical constraints on cells. As a matter of fact, even at low paddle motion (i.e., 30~40 rpm), good homogeneity of the culture medium, total dispersion of the gas phase and effective suspension of microcarriers are observed [5][6][7][8]. Efficient animal cell culture was also showed in this bioreactor for free suspended cells [9] as well as anchorage-dependent cells [10]. Furthermore, as research performed by Goedde et al. [9] highlights, cell concentration and secreted protein production are at least 30% higher with the Nucleo^{TM} disposable bioreactor, as opposed to conventional steel stirred bioreactors under equivalent operating conditions.

Although above performances were experimentally observed, their theoretical basis has yet to be clarified further. Also, the US Food and Drug Administration promotes an approach labelled “Quality by design” [11] in characterising new biotechnological processes. Per said approach, new processes should no longer be developed empirically but on the basis of robust models which represent as closely as possible the physics, the chemistry and the biology involved in the process.

A key step in the development of such a model for the Nucleo^{TM} disposable bioreactor is to get a detailed description of the flow produced by the elliptic pendulum motion of the paddle in the rectangular parallelepiped bag filled with medium culture. Recent flow studies inside other disposable bioreactors show the industrial and scientific interest for this information. Therefore, Nienow et al. [12] have studied by MRF RANS simulation the flow inside ambr^{TM} (TAP Biosystem) which is microscale (15 cm^3) rectangular parallelepiped bioreactor mixed by Elephant Ear impeller. Odeleye et al. [13] investigated by PIV. the flow

in Mobius™ Cell Ready 3 dm³ Bioreactor (Merck Millipore), which looks like a traditional unbaffled stirred tank mixed by a marine propeller. Kaiser et al. [14] simulated, by MRF RANS approach, the flow in BIOSTAT® STR 50 dm³ (Sartorius Stedim) and Univessel® 2 dm³ (Sartorius Stedim); these both disposable bioreactors are mixed by one Elephant Ear impeller and one Rushton turbine. The first disposable bioreactor has however a particular bottom shape while the second disposable bioreactor looks like traditional baffled bioreactor. To mention a last example, Shipman et al. [15] studied par PIV the flow in an oscillatory flow mixer consisting of a pair of flexible chambers connected by a perforated plate. Even if the scientific literature on the subject is continuously increasing, to the authors' best knowledge, no study describing the flow in an equivalent configuration as Nucleo™ disposable bioreactor was published to date. Some publications consider hydrodynamics inside cubic tanks mixed by a conventional impeller, such as a Rushton turbine [16] [17]. Others describe hydrodynamics generated by a pendulum agitator but in these studies, the agitator is moving back and forth [18] and does not draw an elliptic trajectory.

To fill the gap and get relevant information, stereo-PIV measurements were performed in 20 vertical planes covering the whole volume of a 50 dm³ Nucleo™ disposable bioreactor. The flow generated by the paddle motion was characterised for three agitation speeds. Due to the original configuration of the bioreactor, figuring out the exact structure of the flow can be challenging. Current study hence aims at a detailed description of the mean flow within the Nucleo™ bioreactor, which will also help explain performances highlighted in previous studies for the bioreactor.

2. Equipment and methods

2.1 Nucleo™ bioreactor design and agitation conditions

This study covers hydrodynamics inside a 50 dm³ Nucleo™ bioreactor – device is also available in 25 dm³, 250 dm³, 600 dm³ and 1200 dm³ versions. Stereo-PIV is an optical technique, so tank and its contents must be transparent. For this reason, the plastic bag of the Nucleo™ bioreactor is replaced with a same size transparent Plexiglas tank (Table 1).

Table 1: Dimensions of the 50 dm³ Nucleo™ bioreactor.

Bag volume: 50 dm³	Paddle length: 350 mm
Bag length: 430 mm	Paddle width: 140 mm
Bag width: 330 mm	Paddle inclination: 13.5 °
Bag height: 350 mm	Gap with bag bottom: 25 mm
Coefficient of occupancy: 80%	Liquid height: 280 mm

The tank is filled with 40 dm³ of liquid because 80% of the total bag volume corresponds to the maximum coefficient of occupancy usable in animal cell culture. Water is used as a (transparent) liquid model because it shows rheological properties quite similar to culture medium. Three paddle rotational speeds were selected: the first one, equal to 40 rpm, corresponds to the standard condition prescribed for animal cell culture in the 50 dm³ Nucleo^{TM} bioreactor [10]. The two other paddle rotational speeds, equal to 30 rpm and 65 rpm, respectively, are selected in order to appreciate the influence of this parameter on hydrodynamics in the bioreactor.

2.2 Definition of the paddle tip speed and the Reynolds Number

To compute the paddle tip speed and the Reynolds number, characteristic length must be defined. In standard stirred tanks, characteristic length is the impeller diameter, as this length corresponds to the diameter of the cylindrical area covered by the rotating impeller blades. Characteristic length definition is less straightforward for the Nucleo^{TM} bioreactor because the paddle is wide and its external tip draws an ellipse during its rotation (Figure 2). By analogy with definition adopted in standard tanks, we decide to choose, as characteristic length, the size of the major axis *A* of the elliptical trajectory drawn by the external tip of the paddle during its rotation. This characteristic length equals 260 mm. The paddle tip speed V_{tip} and the Reynolds number *Re* are thus defined by equations (1) and (2):

$$V_{tip} = \pi . N . A \quad (1)$$

$$Re = \frac{\rho . N . A^2}{\mu} \quad (2)$$

Their respective values are indicated in Table 2 for the three agitation speeds used in current study. Water density ρ and dynamic viscosity μ, used to compute the Reynolds number *Re*, are equal to 1000 kg.m^{-3} and to 1.10^{-3} Pa.s, respectively.

Table 2: Linear velocity observed at outside tip of the paddle (localized by the white dot on Figure 2) and Reynolds number of the flow for paddle rotational speeds used herein.

paddle rotational speed (rpm)	paddle tip speed (m.s^{-1})	Reynolds number(-)
30 rpm	0.42 m/s	36 450
40 rpm	0.56 m/s	48 600
65 rpm	0.91 m/s	78 975

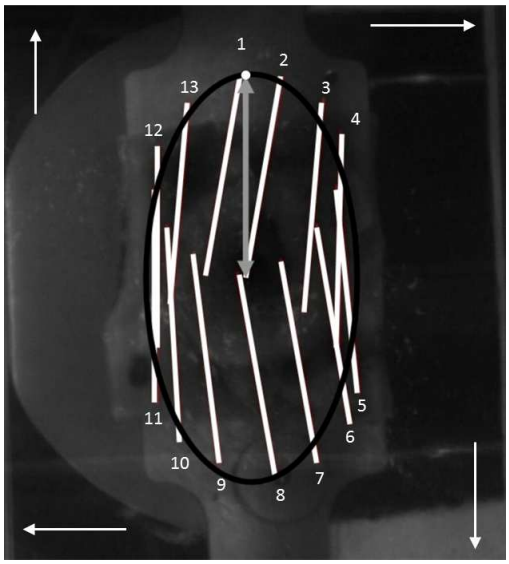

Figure 2: Paddle tip position sequence (white lines) during its rotation, observed through tank bottom. White arrows show direction of paddle displacement in each tank corner. Grey arrow materializes major semi-axis of ellipse swept by the paddle.

2.3 PIV apparatus, parameters and processing

Stereo-PIV is an optical technique which allows measurement of three components of liquid velocity in a bioreactor plane illuminated by a laser sheet. This technique is based on the stereovision principle, just like human vision. Two cameras placed at different angles measure displacement of tracer particles in the plane illuminated by the laser sheet. Data collected by both cameras is then combined to obtain the three velocity components at each point in the measurement plane. More information on the stereo-PIV principle can be found in [19].

The stereo-PIV system used in this study is brought to market by Dantec Dynamics (Denmark). As illustrated in Figure 3, experimental set-up and data acquisition system include:

- A laser Nd-YAG (New Wave Gemini Solo II-30, 532 nm, 2x30 mJ) attached to a sliding rail. This double cavity laser lights up a 3 mm thick plane which may be horizontal or vertical;
- Two Hi/Sense cameras (1280×1024 pixels, 4 Hz) placed at the two ends of a one meter aluminium profile. Each camera is fitted with a Nikon lens (AF Micro Nikkor 60 mm F2.8D) and a Scheimpflug mount. Scheimpflug mount allows camera rotation while lens remains motionless. This mount is necessary to bring all illumination plane points into focus. Experimentally, a 1.5° angle between camera and lens allows reaching this goal. Angle between the two cameras optical axes equals 40°.
- A “timer box” device which synchronizes laser pulsation and camera recording.
- A computer for raw data storage and Dynamic Studio (version 2.30) processing.

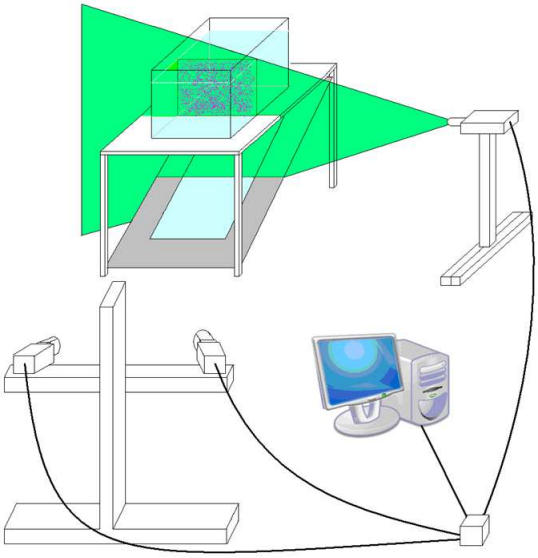

Figure 3: Stereo-PIV apparatus schematic view.

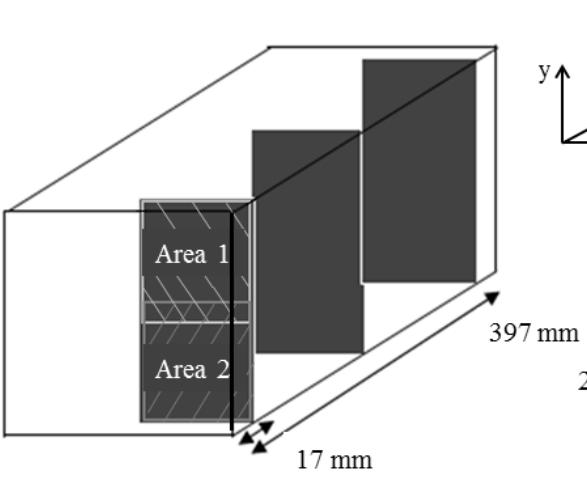

Figure 4 A: Vertical planes selected for stereo-PIV measurements.

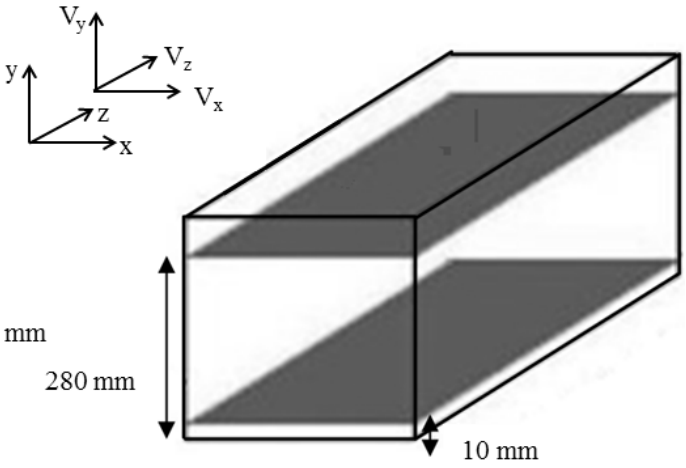

Figure 4 B: Horizontal planes selected for 2D PIV measurements.

Stereo-PIV measurements are performed in 20 vertical planes spaced out by 20 mm. As shown in Figure 4 A, distance between first plane and tank front wall equals 17 mm. 2D PIV measurements are also done in 10 horizontal planes (Figure 4 B) in order to validate out-of-plane velocity component V_z estimated by stereo-PIV in vertical planes. Only one camera is used for 2D PIV measurements, with optical axis perpendicular to the laser plane. Therefore, only velocity components V_x and V_z are measured. As clearance under tank does not allow fitting a PIV camera, a 45° tilted mirror is placed under the tank for 2D PIV measurements (Figure 3). Conventions used throughout this paper for x, y and z axes orientation and components V_x, V_y, and V_z of the velocity vector are specified in Figure 4.

Both for 2D and stereo-PIV measurements, flow is seeded with fluorescent polymer particles (Rhodamine B), whose diameter ranges between 20 and 50 µm and whose density

equals 1190 $kg.m^{-3}$. Particle positions are recorded at 4 Hz on 300 image pairs. Time interval between images of a pair is set between 300 and 7000 µs, depending on paddle rotational speed and numerical processing applied to raw images. For 2D PIV measurements, an instantaneous velocity field is extracted from each image pair by dividing the two images into interrogations areas of 32×32 pixels² with 16 pixels overlap and by applying a cross correlation function in these areas. The spatial resolution of these 2D velocity fields equals 7 mm. For stereo-PIV measurements, an adaptive correlation function is separately applied on images recorded by each camera. Initial and final interrogation areas cover 64×64 $pixels^2$ and 16×16 $pixels^2$, respectively, with 50% overlap in both cases. Stereo instantaneous velocity fields are then reconstructed from instantaneous velocity fields obtained for each camera and from a polynomial model which accounts for camera orientation and distance relative to measurement plane. For each vertical measurement plane, polynomial model parameters were estimated by placing a 5 mm square grid pattern in the plane, with 2 mm black dots where lines intersect. To obtain a 1 mm spatial resolution velocity field with a camera sensor size equal to 1024×1208 pixels², stereo-PIV measurements must be performed in two steps to cover the whole liquid height. For these two steps, cameras were successively focused on rectangular areas illustrated in Figure 4 A (areas 1 and 2).

Mean velocity field is then computed from the 300 instantaneous velocity fields. However, paddle leaves a shadow on image when crossing the laser plane. Velocity vectors computed in this shadow area are mostly irrelevant. Shadow area is therefore identified in each image to define a mask applied to each instantaneous velocity field. Irrelevant instantaneous velocity vectors are thus excluded from mean velocity field computation.

3. Results and discussion

3.1 Mean flow pattern

Due to the elliptical trajectory drawn by the paddle during its rotation, a symmetry inside the mean velocity flow is expected. To identify this symmetry is interesting to determine the minimal part of the tank which is representative of the whole flow and may be thus used to analyse the mean velocity field. Figure 2 shows rotating paddle position sequence when observed through tank bottom and reveals paddle tip does not remain parallel to tank side during rotation. Therefore, mean velocity flow has no rotational symmetry. Nevertheless, analysis of horizontal 2D mean velocity fields does highlight symmetrical flow in tank opposite quarters. Figure 5 illustrates this central axis symmetry through a horizontal cross-section of mean velocity field at 10 mm from tank bottom. Background grey levels (see colour scale)

show values of the modulus of velocity components V_x and V_z normalized by paddle tip speed: $\sqrt{V_x^2 + V_z^2}/V_{tip}$. Black arrows indicate velocity vectors orientation. Velocity orientation highlights central axis symmetry while velocity magnitude distribution shows slightly smaller values for tank left side, which results from laser placement to the right of the tank during horizontal 2D PIV measurement. Indeed, tank left side is frequently shadowed by paddle. Mean velocity field in tank left side is therefore computed from less instantaneous velocity vectors, as irrelevant (shadowed) ones are systematically excluded by processing described in last paragraph of section 2.3. As this discrepancy arises from data processing itself, it may be concluded to symmetrical flow in tank opposite quarters and the mean velocity fields can thus be only analyzed in the half right part of it.

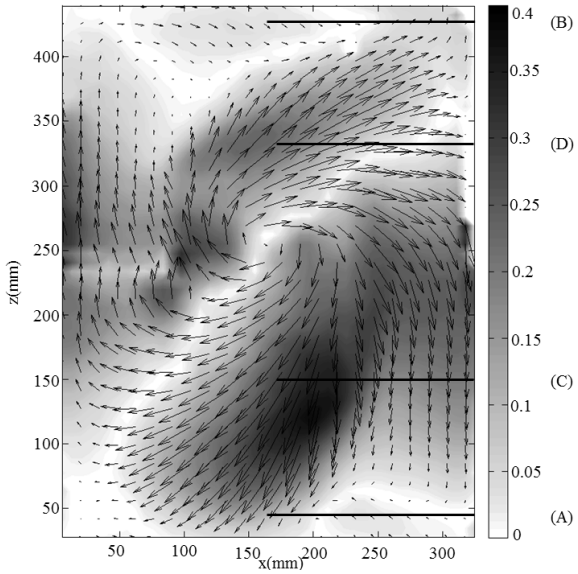

Figure 5: 2D mean velocity field obtained in the horizontal plane localized at 10 mm from the bottom tank when the paddle rotates at 40 rpm. For the picture clarity, one vector on two is plotted. Black lines and Symbols A, B, C, D locate vertical measurement planes corresponding to stereo PIV measurements of the Figure 8.

Mean flow pattern can schematically be described as a three-dimensional helix coiled on itself to form a distorted horizontal torus (Figure 6). Helix loops are revealed through vertical stereo mean velocity fields analysis while torus outline can be observed through horizontal 2D mean velocity fields. Figures 7 A-D display vertical stereo mean velocity fields in tank right half. As illustrated in Figure 5, measurement planes in Figures 7 A and 7 B are adjacent to front and back tank walls (z=17 mm and 397 mm, respectively) while measurement planes in Figures 7 C and 7 D are centred in front and back quarters of tank right half (z =137 mm and 317 mm, respectively). Vertical velocity vectors in these figures show that, on average, fluid particles go up along the tank wall and go down in the area swept by the paddle, therefore drawing helix loops. Horizontal 2D mean velocity fields in Figure 5 (y=10 mm) and

Figures 8 A-B (y = 100 mm) show clockwise rotation of liquid flow around tank centre. Moreover, Figures 8 A and B, where background grey levels relate to intensity of velocity components V_x and V_z, respectively, highlight that these components exhibit maximum values in specific and different areas (see boxes). Each part of the tank is thus characterized by a specific flow direction which corresponds to paddle displacement main orientation in each area (Figure 2).

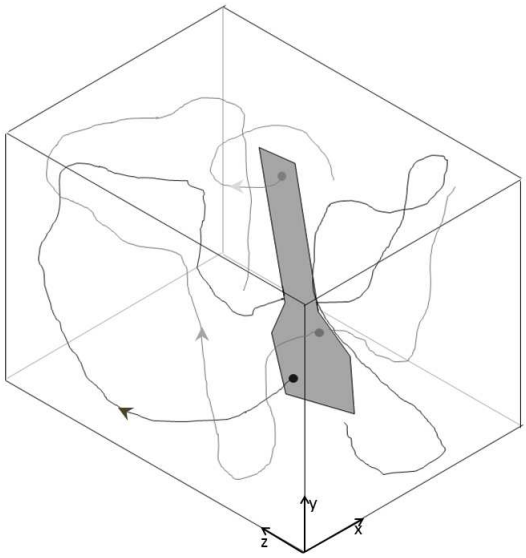

Figure 6: Schematic representation of mean flow pattern followed by fluid particles inside tank.

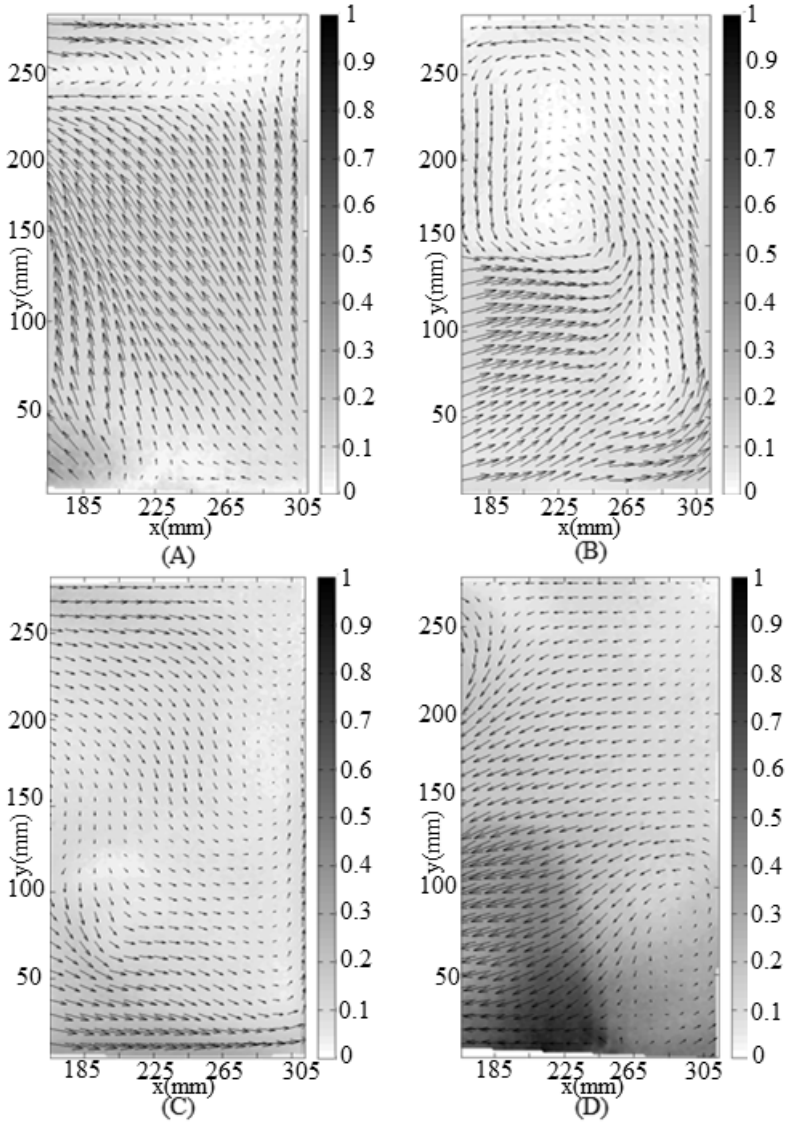

Figure 7: Vertical stereo mean velocity fields in the half right part of the tank (i.e the right image boundary corresponds to the tank wall and the left one is the center of the tank). The background color is the normalized velocity vector magnitude $\sqrt{V_x^2 + V_y^2 + V_z^2}/V_{tip}$ when the paddle rotates at 40 rpm. The arrows are the projection of the velocity vectors in the measurement plane localized (A) 17 mm (B) 397 mm (C) 137 mm (D) 317 mm from the front tank wall. For picture clarty, one vector on ten is plotted.

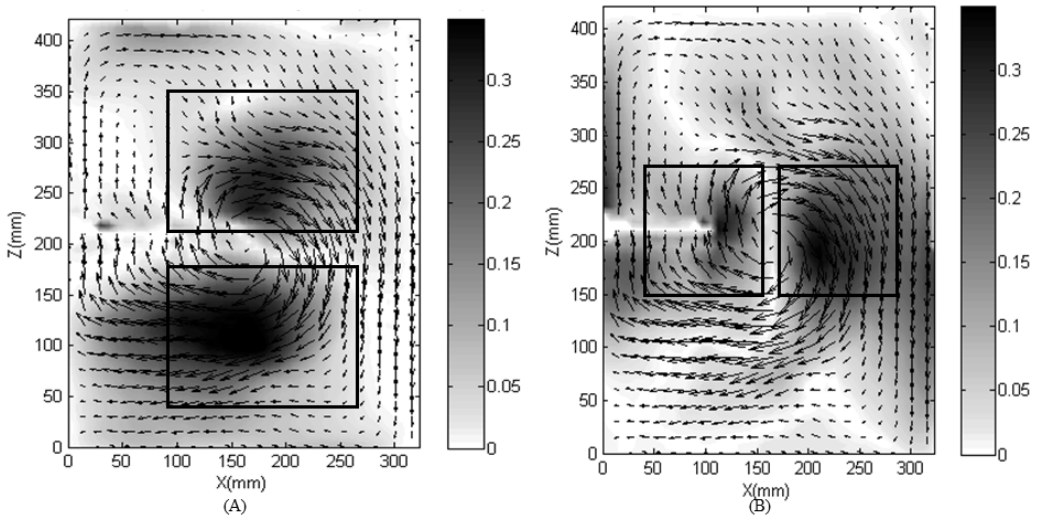

Figure 8: Spatial distribution of the normalized velocity component V_x/V_{tip}(Fig 10A) and of the normalized velocity component V_z/V_{tip} (Fig 10 B). The paddle rotational speed is 40 rpm and the measurement plan is distant to 100 mm from the tank bottom. For picture clarty, one vector on two is plotted.

3.2 Spatial distribution of mean velocity components

Mean flow inside the Nucleo™ bioreactor is therefore fully three-dimensional. Moreover, no stagnant area is observed in tank corners, unlike suggested by its rectangular parallelepiped shape. Mean flow in right front and back corners is illustrated in Figures 9 A-B and Figures 10 A-B, respectively. Background grey levels on these figures relate to intensity of velocity components belonging to measurement plane ($\sqrt{V_x^2+V_y^2}/V_{tip}$, Figure A) and of velocity component normal to measurement plane (V_z/V_{tip}, Figure B), respectively. In each tank corner, flow is not stagnant because fluid particles have minimum mean velocities as high as 5% of paddle tip speed V_{tip} (5% of 560 mm/s). Also, flow is mainly oriented according to *z* axis in tank right front corner, while it is mainly oriented according to *x* axis in tank right back corner. These flow orientations in each corner are again in accordance with paddle main displacement direction near these corners (Figure 2).

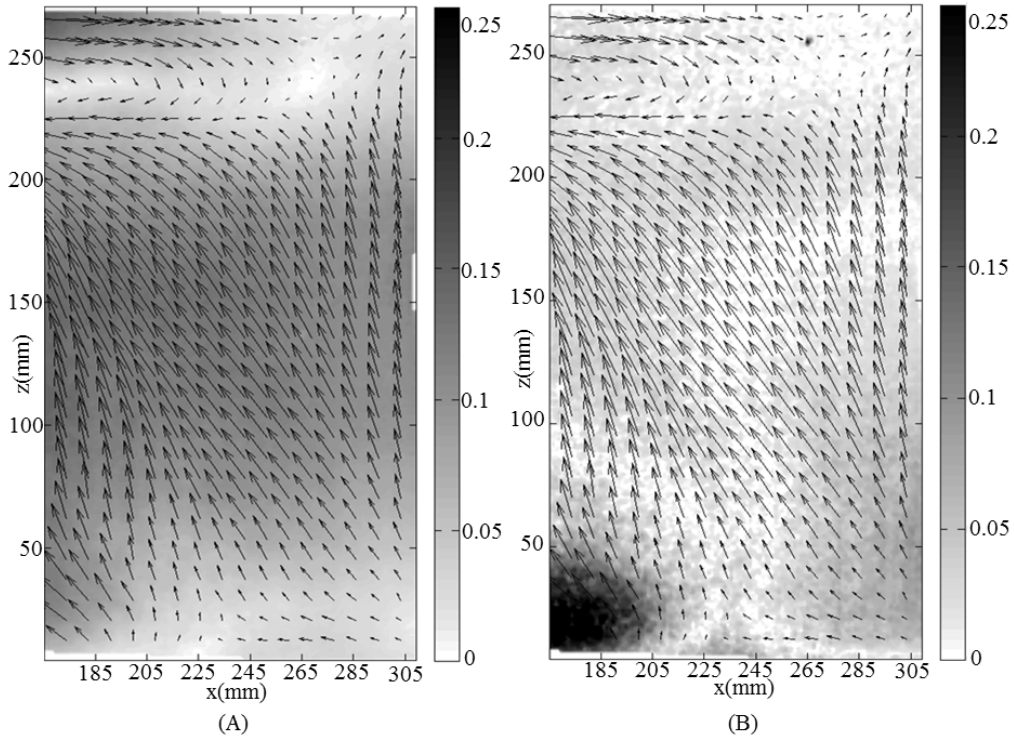

Figure 9: (A) Spatial distribution of the modulus of velocity components V_x and V_y divided by the paddle tip speed $\sqrt{V_x^2+V_y^2}/V_{tip}$ (B) Absolute value of the normalized z-velocity component $|V_z|/V_{tip}$ in the front right corner of the tank (z=17 mm) for the paddle speed equals 40 rpm. For picture clarty, one vector on ten is plotted

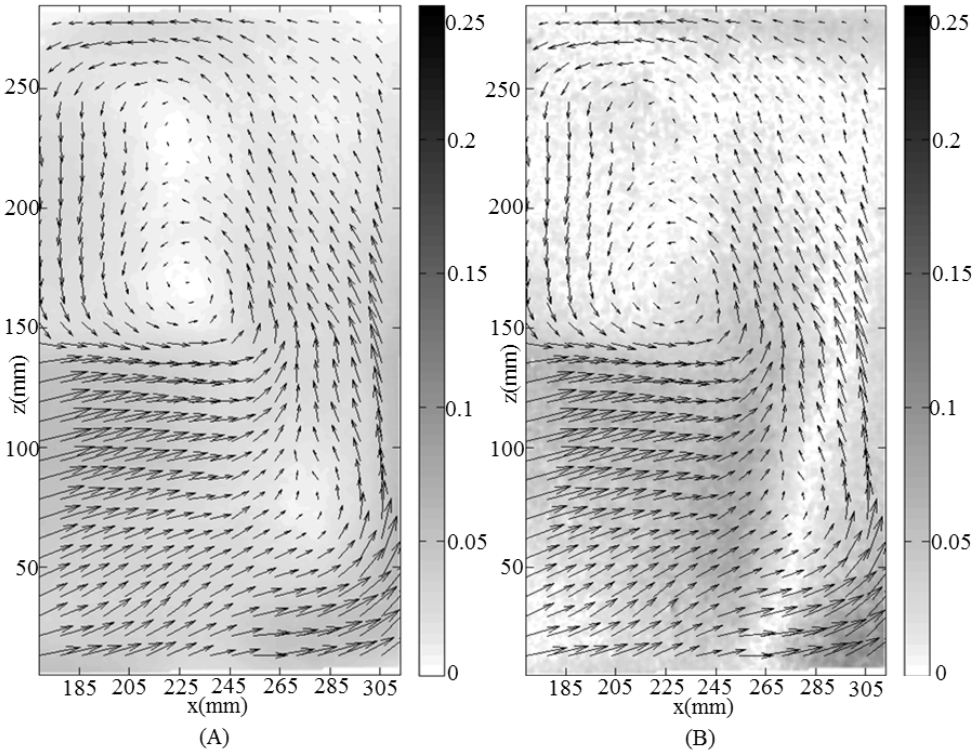

Figure 10 : (A) Spatial distribution of the modulus of velocity components V_x and V_y divided by the paddle tip speed $\sqrt{V_x^2 + V_y^2}/V_{tip}$ (B) Absolute value of the normalized z-velocity component $|V_z|/V_{tip}$ in the back right corner of the tank (z=397 mm) for the paddle speed equals 40 rpm. For picture clarty, one vector on ten is plotted.

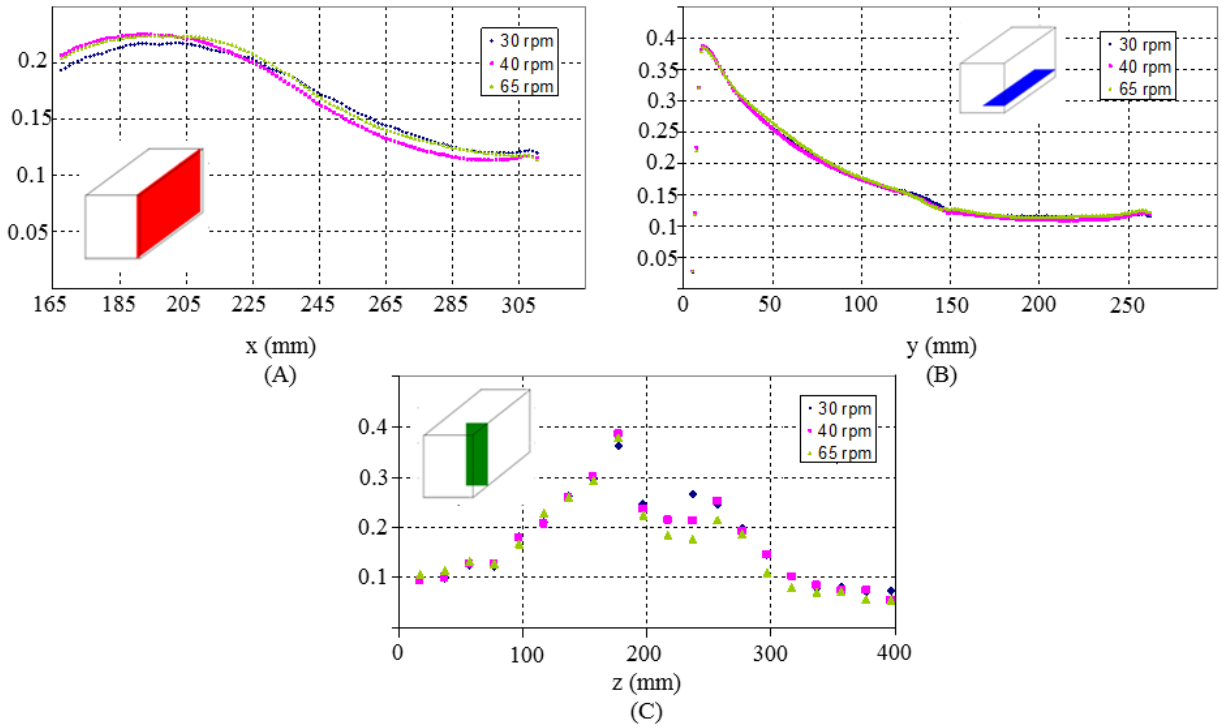

Figure 11: Profile for spatial average of normalized mean velocity magnitude ($\sqrt{V_x^2 + V_y^2 + V_z^2}/V_{tip}$) measured in tangential (Fig. 11 A), horizontal (Fig. 11 B) and vertical (Fig. 11 C) planes, respectively.

Although flow is not stagnant in tank corners, mean velocity is clearly higher in cone swept by the paddle, as illustrated in Figures 11 A-C, where each point shows an average value of normalised mean velocity $\sqrt{V_x^2 + V_y^2 + V_z^2}/V_{tip}$ in a tank plane (A = tangential plane, B = horizontal plane, C = vertical plane). Each profile corresponds to average values measured in a series of parallel planes. In the *x*-direction (from left to right), paddle swept an area extending up to a 80 mm maximum distance from tank centre. As shown in Figure 11 A, normalised mean velocity is 1.5 to 2 times higher in this area. In the *y* direction (from bottom to top), normalised mean velocity gradually decreases as distance from tank bottom increases, until reaching a minimum and stable value when *y* exceeds 150 mm (Figure 11 B). This profile in two parts is due to the paddle specific shape (Figure 1), which consists in a wide trapezoidal blade in its lower part and a straight narrow shaft in its upper part. In *z* direction (from front to back), normalised mean velocity increases from tank walls to tank centre (Figure 11 C), except for a small decrease in measurement plane at tank middle length (z = 217 mm; tank length = 430 mm). This singularity arises from the fact that each mean velocity field is computed from instantaneous velocity fields recorded for all paddle positions. As illustrated in Figure 12 A, paddle sweeps tank middle from left to right or right to left depending on its position. In median vertical measurement plane (z = 217 mm), some instantaneous velocity fields thus have vectors oriented to the left (Figure 12 B) and others have vectors oriented to the right (Figure 12 C). When mean velocity field is computed from an arithmetic mean, magnitudes of these opposite vectors partly neutralize each other. Apart from above singularity, main conclusion is that mean velocity average magnitude is almost twice higher in area swept by the paddle.

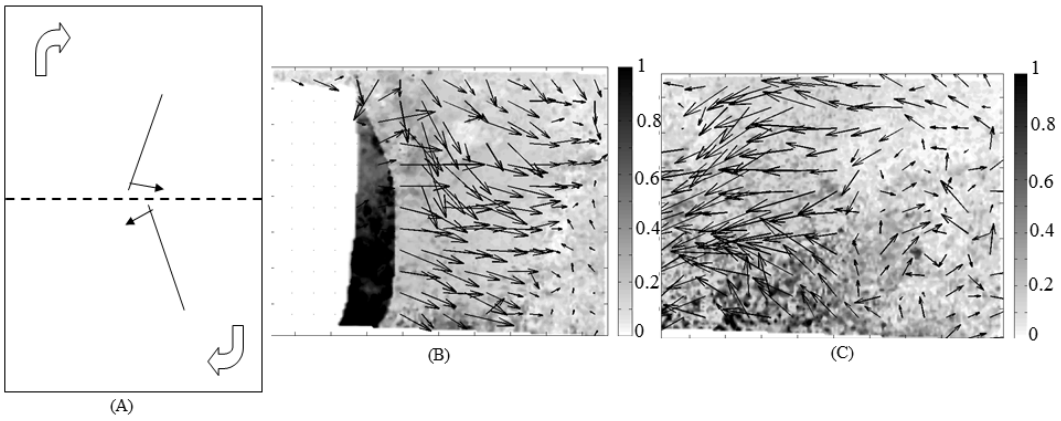

Figure 12: (A) Paddle sweeps tank median plane from left to right and from right to left depending on its position. (B) Instantaneous velocity field obtained in this median plane (z = 217 mm). This instantaneous velocity field corresponds to area 2 of stereo PIV measurement. Paddle is in tank front half. Flow is mainly oriented from left to right. (C) Instantaneous velocity field obtained when paddle is in tank back half, opposite to position in Figure 12 B. Flow is mainly oriented from right to left. For picture clarty, one vector on ten is plotted.

3.3 Numerical distribution of mean velocity components

In addition to mean flow spatial distribution, numerical distribution is showed in Figure 13, with distribution percentiles listed in Table 3. These figures are worked out from mean stereo velocity fields measured in 20 vertical planes. Therefore, these numerical distributions do not correspond to volume percentage relative to the whole tank volume. They actually correspond to a surface percentage. However, as the 20 vertical planes are equally distributed along tank volume, numerical distributions worked out based on these planes should properly approximate real distribution, i.e. distribution that would be computed if data was available for the whole tank. Mean flow numerical distribution (Figure 13-A) exhibits two maxima, the main one for abscissa 0.08 V_{tip} and the second one for abscissa 0.3 V_{tip}. As discussed in section 3.2, these values correspond to ranges encountered outside and inside paddle swept volume. Despite these two ranges of values, mean velocity numerical distribution remains quite narrow, as 95% of measurement planes total surface has a velocity ranging from 0 to 0.43 V_{tip}. Distributions for *x*- *y*- *z*- velocity components are drawn considering their absolute values so as to ease comparison. Two kinds of distributions are obtained: on the one hand, V_x and V_z velocity components distributions which exhibit similar shapes except for highest values (Figures 13 B and D) and, on the other hand, V_y velocity component distribution which is comparatively twice narrower (Figure 13 C). As a consequence, flow is more intensive in the horizontal direction compared to the vertical one. Nevertheless, even if V_y velocity component distribution is narrow, its range of values remains significant when compared to tank size. For instance, a fluid particle moving at median velocity (0.038 V_{tip}) takes on average 13 s to travel a distance equal to liquid height (280 mm) with paddle rotating at 40 rpm. Therefore, flow can still be considered as fully three-dimensional with a preferential orientation inside horizontal planes.

Table 3: Percentiles of normalized mean velocity numerical distribution (-) and of normalized V_x, V_y, V_z velocity components absolute value (-).

	P_{25}	P_{50}	P_{75}	P_{90}	P_{99}
$\sqrt{V_x^2 + V_y^2 + V_z^2}/V_{tip}$	0.075	0.117	0.218	0.346	0.831
$\lvert V_x \rvert / V_{tip}$	0.027	0.057	0.110	0.211	0.314
$\lvert V_y \rvert / V_{tip}$	0.019	0.038	0.067	0.095	0.144
$\lvert V_z \rvert / V_{tip}$	0.026	0.060	0.140	0.268	0.816

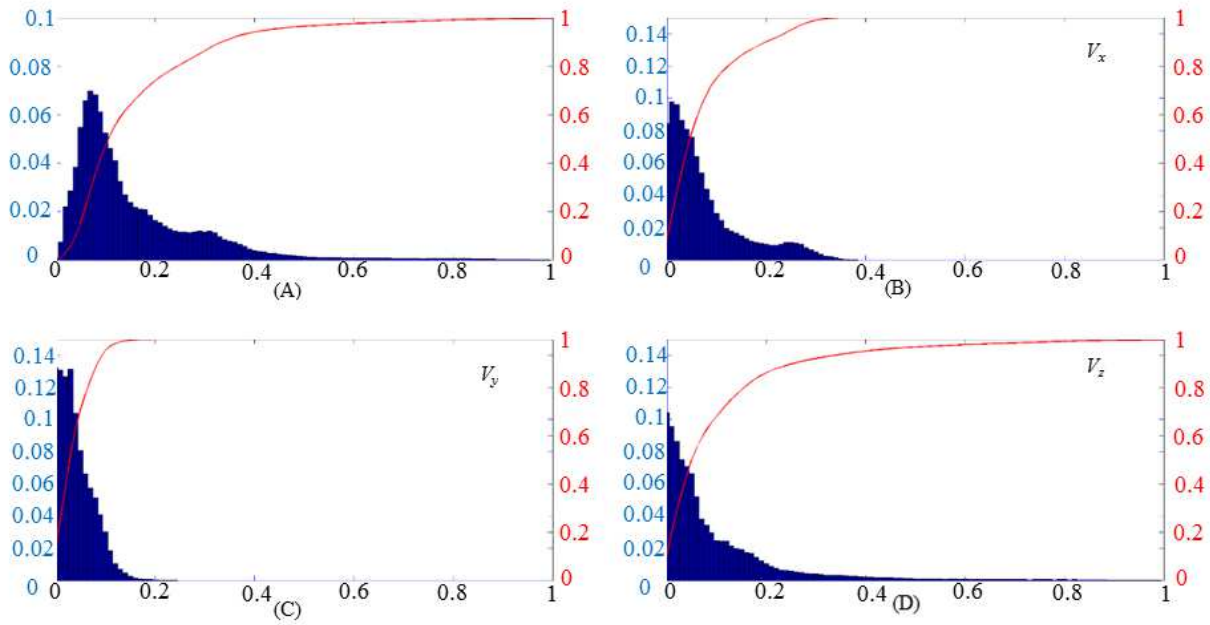

Figure 13: (A) Normalized mean velocity numerical distribution in 20 vertical measurement planes (B-C-D) Normalized V_x, V_y, V_z-velocity components absolute value distribution.

Flow inside tank should be turbulent, as Reynolds number values *Re* (Table 2) computed for agitation conditions (30 rpm, 40 rpm and 65 rpm respectively) used in current study significantly exceed 10 000. Hypothesis is confirmed by analysis of the stereo mean velocity flow measured at the above paddle rotational speeds. Indeed, as shown in Figures 11 A-C, mean normalised velocity profiles computed for the three agitation conditions overlap perfectly. Independence between these dimensionless velocity fields and paddle rotational speed is a fundamental feature of turbulent flow. In other words, all observations relating to mean flow structure remain valid for any paddle rotational speed, provided that this speed is high enough to maintain flow turbulence.

3.4 Comparison of the flow structure generated in Nucleo™ bioreactor with conventional baffled and unbaffled stirred bioreactor used for animal cell culture

The flow generated inside the Nucleo™ bioreactor shares some characteristics with those produced in conventional baffled and unbaffled stirred bioreactor. Indeed, as shown by the works of Collignon et al. [20], Zhu et al. [21] , for instance, which described by PIV the mean flow inside conventional baffled stirred bioreactor mixed by axial propeller as Elephant Ear impeller, the flow is turbulent and its dimensionless velocity field is independent of the impeller rotational speed as in the Nucleo™ bioreactor. Moreover, the mean velocity is either higher in the area next to the propeller and is smaller in the rest of the tank. However, the mean velocity seems more homogeneously distributed in the Nucleo™ than in conventional

baffled stirred bioreactor thanks to the large area of the tank swept by the paddle. Finally, the previous numerical comparison of velocity components V_x , V_y ,V_z distribution (section 3.3) highlights the flow structure in the Nucleo^{TM} bioreactor is an hybrid between the flow structure inside convention baffled and unbaffled stirred bioreactor. Indeed, as shown by works of Alcamo et al. [22], the flow in unbaffled stirred tank is more intensive in horizontal direction than in vertical one while, in baffled stirred tank, it is more intensive in vertical direction than in horizontal one. In the Nucleo^{TM} bioreactor, it is twice intensive in horizontal direction than in vertical one however this latter remains significant. This hybrid behaviour is due to the rectangular parallelepiped shape of the tank where the corners partially play the baffle role. As many disposable bioreactors are not equipped with baffles for reasons of easy manufacturing plastic bags, this hybrid behaviour combined with a more or less homogeneous distributions of the velocity field give an advantage to Nucleo^{TM} bioreactor, especially in process where solid phase must be kept in suspension, as in the culture of anchorage dependant animal cell on microcarriers.

4. Conclusion

Current study offers unprecedented mean flow characterisation for the original design of the Nucleo^{TM} bioreactor and further explains performances experimentally observed in previous studies for mixing, solid suspension and animal cell culture. Characterized flow pattern can be described as a three-dimensional helix coiled on itself to form a distorted horizontal torus which covers the whole tank volume. Despite mean velocity values twice higher in cone swept by paddle and horizontal velocity components twice the vertical one, mean velocity remains significant everywhere and no stagnant area is observed in tank corners. Moreover, flow turbulence is reached even at low impeller rotational speeds, which means enhanced mixing capacity and invariance of the dimensionless mean velocity field per paddle rotational speed. All observations performed in current study therefore remain valid for other paddle rotational speeds.

This unprecedented study of hydrodynamics in the Nucleo^{TM} bioreactor paves the way for ample further research. Firstly, as the flow is turbulent, it should be very interesting to study the spatial and numerical distribution of quantities associated to the turbulence and computed from the time fluctuating component of the velocity, as the turbulent kinetic energy k and its dissipation rate ε. Mechanical constraints inside the flow could be evaluated from these turbulent proprieties and compared to those obtained in conventional bioreactors, so as to better clarify why cell concentration and secreted proteins production are significantly higher in the

Nucleo™ bioreactor [9]. Secondly, all PIV experimental data offer quite useful resources for the validation of CFD simulations, the latter offers the advantage to quantify the 3D flow is in the whole tank volume. Finally, a complementary Lagrange approach could be superimposed on the Euler approach adopted in current study, as the cartography of the mean velocity field has been established. A Lagrange approach, which consists in tracing one particle in the tank, could give information on the local environment (concentration, mechanical constraints, etc.) met by an animal cell, as a function of time. Frequency, duration and level of mechanical constraints, for instance, could be computed and compared with outcomes in conventional bioreactors.

Notations

A	major axis size for ellipse drawn by paddle external tip
k	turbulent kinetic energy ($m^2.s^{-2}$)
N	paddle rotational speed (rpm)
Re	Reynolds number (-)
V_{tip}	linear velocity at paddle external tip ($m.s^1$)
V_x, V_y, V_z	Velocity components along *x, y and z* axes, respectively
x,y,z	Cartesian axes aligned along vessel walls
ε	dissipation rate of kinetic energy ($m^2.s^{-3}$)
μ	dynamic viscosity (Pa.s)
ρ	fluid density ($kg.m^{-3}$)
rpm	rotation per minute
PIV	Particle Image Velocimetry

Acknowledgements

We acknowledge the FRS-FNRS (National Fund for Scientific Research of Belgium) for its financial support via M.-L. Collignon's research fellow grant. (research agreement 1120208F) and her postdoctoral researcher grant (research agreement 1206614F).

References

[1] R. Eibl, D. Eibl, Application of disposable bag bioreactors in tissue engineering and for the production of therapeutic agents, Advances in Biochemical Engineering and Biotechnology 112 (2009) 183-207. (DOI 10.1007/10_2008_3)

[2] M. Pietrzykowski, W. Flanagan, V. Pizzi, A. Brown, A.Sinclair, M. Monge, An environmental life cycle assessment comparison of single use and conventional process technology for the production of monoclonal antibodies. Journal of Cleaner Production 41 (2013) 150-162.

[3] R.S. Cherry, E.T. Papoutsakis, Hydrodynamic effects on cells in agitated tissue culture reactors. Bioprocess Engineering 1 (1986) 29-41. (DOI 10.1007/BF00369462)

[4] M.S. Croughan, J.F.P Hamel, D.I.C Wang, Effects of microcarrier concentration in animal cell culture. Biotechnology and Bioengineering 32 (1988) 975-982. (DOI: 10.1002/bit.260320805)

[5] Newmix-Levteck application note, 2008 a. Demonstrating temperature uniformity in cubical mix bag with pad-drive™. http://www.atmi.com/ls-assets/pdfs/new_mix/pad_drive/paddrive_demonstrating_temperature_uniformity_in_cubical_mix_bags_rev1.pdf viewed February 4, 2014.

[6] Newmix-Levteck application note, 2008 b. Mixing uniformity in cubical mixing bags with pad-drive™. http://www.atmi.com/ls-assets/pdfs/new_mix/pad_drive/pad-drive_mixing_uniformity_rev2.pdf viewed February 4, 2014).

[7] Nucleo™ application note, 2010. Microcarrier mixing: stirring speed effect on Cytodex suspension in Nucleo™ Single-Use bioreactor. No anymore available on the website of ATMI LifeSiences. Downloaded in 2010

[8] SoloHill application note, 2012. Integrity™ PadReactor. SoloHill microcarriers in a 25L PadReactor Single-Use Bioreactor. http://www.atmi.com/ls-assets/pdfs/Bioreactors/padreactor/PadReactor_SoloHill_AppNote.pdf viewed February 4, 2014.

[9] A. Goedde, S. Reiser, O. Krüger, A. Cayli, K. Russ, Characterization of two single-use bioreactors for mammalian cell culture processes. Biomanufacturing Summit, January 26, 2010. San Diego. USA.

[10] J. Castillo, S. Vanhamel, Cultivating anchorage-dependent cells. Disposable bioreactor can grow animal cells immobilized on microcarriers. Genetic Processing and Biotechnologyy news 27 (2007) 40-41.

[11] FDA guidance for industry, 2004. Sterile drug products produced by aseptic processing-current good manufacturing practice. http://www.fda.gov/downloads/Drugs/.../Guidances /ucm070342.pdf viewed February 4, 2014.

[12] A.W. Nienow, C.D. Rielly, K. Brosnan, N. Bargh, K. Lee, K. Coopman, C. Hewitt, The physical characterisation of a microscale parallel bioreactor platform with an industrial CHO cell line expressing an IgG4. Biochemical Engineering Journal 76 (2013) 25-36. (DOI: 10.1016/j.bej.2013.04.011)

[13] A.O.O. Odeleye, D.T.J Marsh, M.D Osborne, G.J. Lye, M. Micheletti, On the fluid dynamics of a laboratory scale single-use stirred bioreactor. Chemical Engineering Science 111 (2014) 299-312. (DOI: 10.1016/j.ces.2014.02.032)

[14] S.C. Kaiser, C. Loffelholz, S. Werner, D. Eibl, CFD for characterizing standard and single use stirred cell culture bioreactors, Computational fluid dynamics technologies and applications, Prof Igor Minin (Ed.) ISBN 978-953-307-169-5. In Tech.

[15] T.N. Shipman, A.K. Prasad, S.L. Davidson, D.R. Cohee, Particle image velocimetry evaluation of a novel oscillatory-flow flexible chamber mixer. Journal of Fluids Engineering 129 (2007) 179-187. (DOI: 10.1115/1.2409347)

[16]J. Kilander, F.J.E. Svensson, A. Rasmuson, Flow instabilities, energy levels and structure in stirred tanks. AIChE Journal 52 (2006) 4039-4051. (DOI: 10.1002/aic.11036)

[17]O.P. Prat, J.J. Ducoste, Simulation of flocculation in stirred vessels, Lagrangian versus eulerian. Chemical Engineering Research and Design 85(2007) 207-219. (DOI: 10.1205/cherd05001)

[18] S. Masiuk, J. Kawecka-Typek, Mixing energy measurements in liquid vessel with pendulum agitators. Chemical Engineering and Processing 43 (2003) 91-99. (DOI: 10.1016/S0255-2701(03)00072-2)

[19] A.K. Prasad, Stereoscopic particle image velocimetry. Experiments in Fluids 29 (2000) 103-116. (DOI 10.1007/s003480000143)

[20] M.L. Collignon, A. Delafosse, M. Crine, D. Toye, Axial impeller selection for anchorage dependant animal cell culture in stirred bioreactors: Methodology based on the impeller comparison at just-suspended speed of rotation. Chemical Engineering Science 65 (2010) 5929-5941. (DOI: 10.1016/j.ces.2010.08.027)

[21] H. Zhu, A.W. Nienow, W. Bujalski, M.J.H Simmons, Mixing studies in a model aerated bioreactor equipped with and up- or a down-pumping 'Elephant Ear' agitator: Power, hold-up and aerated flow field measurements. Chemical Engineering Research and Design 87 (2009) 307-317. (DOI: 10.1016/j.cherd.2008.08.013)

[22] R. Alcamo, G. Micale, F. Grisafi, A. Brucato, M. Ciofalo, Large-eddy simulation of turbulent flow in an unbaffled stirred tank driven by a Rushton turbine. Chemical Engineering Science 60 (2005)2303-2316. (DOI: 10.1016/j.ces.2004.11.017)